Clim Dyn (2016) 47:3613–3626
DOI 10.1007/s00382-016-3031-9

Comparison between high-resolution climate simulations using single- and double-nesting approaches within the Big-Brother experimental protocol

Dominic Matte[1] · **René Laprise**[1] · **Julie Mireille Thériault**[1]

Received: 4 July 2015 / Accepted: 10 February 2016 / Published online: 26 February 2016

Abstract Regional climate models (RCM) are widely used to downscale global climate models' (GCMs) simulations. As the resolution of RCM increases faster than that of GCM used for climate-change projections till the end of this century, the resolution jump will become an issue. Cascade with multiple nesting offers an approach to reach high resolution while keeping reasonable computational cost. Few studies have addressed whether the best results are obtained with the single- or multiple-nesting approaches. In this study the results obtained with single and double nesting are compared within the idealised "perfect model" framework of the Big-Brother Experiment. This method consists in first realizing a simulation, nicknamed the Big-Brother (BB) simulation, on a relatively large domain at the desired resolution, to serve as reference dataset. The BB results are then processed by a low-pass filter to emulate a coarse-resolution dataset to be used as LBC to drive further simulations, nicknamed the Little-Brother (LB) simulations, using an identical model formulation and resolution as the BB simulation. For the single nesting, the LB simulations are directly simulated, while for the double nesting a surrogate intermediate-resolution simulation is used. The study of the time-mean (stationary) component shows that little difference is noted between the single- and double-nesting approaches. The time-deviation (transient-eddy) component, however, shows important differences. The double-nesting approach weakly degrades the large scales but allows a significant reduction of the required domain size to allow adequate spin-up of fine-scale features. This results in an important saving in the computational cost.

Keywords High-resolution climate simulation · Big-Brother experiment · Multiple dynamical downscaling · Spatial spin-up

1 Introduction

General Circulation Models (GCMs) are widely used for climate-projection studies; their heavy computational cost rapidly becomes an issue if one attempts increasing their resolution. The use of nested limited-area regional climate models (RCMs) to dynamically downscale GCM output allows drastically reducing the computational cost while benefiting from the added value related to the increased resolution. With very fine grid meshes, however, the computational cost of an RCM also becomes an issue. Over the recent years, several groups have embarked upon the production of very high spatial resolution, and even convection-permitting climate simulations (e.g. Hohenegger et al. 2008; Chan et al. 2012; Lauwaet et al. 2013; Ban et al. 2015; Prein et al. 2015) and climate-change projections (e.g. Trapp et al. 2007; Pavlik et al. 2012; Kendon et al. 2014) using multiple grid nesting. Such simulations indicate great perspectives for added value of high-resolution climate simulations. For example, de Vries et al. (2014) used a mesh of 12 km to study changes of mean snowfall and seasonal extremes. Jacob et al. (2014) presented the first high-resolution (12.5 km grid mesh) future climate projections of EURO-CORDEX. They highlighted a clear change of pattern of heavy precipitation events compared to coarser simulations. Kendon et al. (2012) pointed out that 12 km grid mesh is still too coarse to give a realistic

✉ Dominic Matte
mattedominic3@gmail.com

[1] Centre ESCER, Department of Earth and Atmospheric Science, Université du Québec à Montréal (UQAM), Downtown Station, P.O. Box 8888, Montréal, QC H3C 3P8, Canada

spatial and temporal structure of heavy rain, suggesting convection-permitting 1.5 km grid-mesh simulation for improvement.

Cholette et al. (2015) have shown that with grid meshes of 1–3 km, the fifth-generation Canadian Regional Climate Model (CRCM5) showed a clear improvement in the simulation of wind channelling effect in the St. Lawrence River Valley located in Québec, Canada. The study of Wang et al. (2013) revealed that high resolution improves local features such as sea breezes and funnelling winds in the Met Office United Model (MetUM) RCM. In the case of simulations over complex topography with the Weather Research and Forecasting (WRF) RCM version 3.0, Rasmussen et al. (2011) have shown that spatial snowfall distribution is much more representative of observations with 2 km than 36 km grid-mesh simulations; they attributed this result to a more realistic vertical motion at higher resolution.

Recently, Kjellström et al. (2014) had put forward that international cooperation is important to reinforce our knowledge about very high-resolution regional climate modelling. Two of the central issues of dynamical downscaling are the regional domain size and the resolution jump between the driving lateral boundary conditions (LBC) and the nested RCM grid mesh, both issues being interrelated. For example, Jones et al. (1995) have shown that the domain size should be large enough to allow the full development of fine scales but small enough to maintain suitable control by the LBC on the regional simulation. Using the Big-Brother Experiment (BBE) protocol, Leduc and Laprise (2009) and Leduc et al. (2011) have shown that a minimum distance from the lateral inflow boundary is required for the suitable development of small-scale transient-eddy permitted by the fine mesh of a RCM. This spatial spin-up distance is particularly large for mid-latitude winter conditions characterized by strong westerly flow. The spatial spin-up imposes a non-negligible constraint on the domain size, which has repercussions on the computational cost. While domain size and spatial spin-up have been studied in several studies, its relation to resolution jump is poorly known; practitioners of dynamical downscaling, however, are fully aware that larger jumps exacerbate the spin-up issue. Recently, Di Luca et al. (2015) have discussed some of the important factors influencing the added value brought by RCM using multiple dynamical downscaling. They raised the point that even if the grid mesh could be reduced substantially, errors from the nesting may limit its application. In order to keep the computational cost low, Brisson et al. (2015) have investigated different nesting approaches to perform convection-permitting climate simulations on a 0.025° mesh. They compared simulations performed with single nesting (0.025°-mesh simulation performed using directly ERA-Interim as initial conditions (IC) and LBC), double nesting (an intermediate-resolution on a 0.22° mesh between ERA-Interim and the 0.025°-mesh simulation) or triple nesting (two intermediate-resolution on a 0.22° and 0.0625° mesh simulations between ERA-Interim and the 0.025°-mesh simulation). Their results suggested that the intermediate-resolution 0.0625°-mesh simulation does not make a significant impact and that this nest could therefore be removed. They also mentioned that single nesting increased model deficiencies. However, it remains unclear what is the impact of a multiple dynamical downscaling approach. Hitherto, it is not well understood how a multiple nesting approach affects high-resolution climate simulations. To the best of the authors' knowledge, no study has yet addressed this issue.

This paper investigates dynamical downscaling in situations of large resolution jump between the driving LBC and the RCM grid mesh, by comparing the performance of single and double nesting approaches, using the BBE protocol. It is constructed as follows. A brief description of the regional model is presented in Sects. 2, 3 and 4 discuss experimental design and the analysis tools used to analyze the simulations. The results are presented in Sect. 5. Finally, Sect. 6 presents the summary and discussions.

2 Model description

The experiments have been performed with the fifth-generation Canadian RCM (CRCM5; Hernández-Díaz et al. 2013; Martynov et al. 2013; Šeparović et al. 2013). CRCM5 is based, in large part, on the Global Environmental Multiscale model [GEM; Côté et al. (1998a, b)] developed by Environment Canada for use in numerical weather prediction (NWP). The dynamical core uses a two-time-level quasi-implicit semi-Lagrangian marching scheme, and the horizontal discretization is based on an Arakawa staggered C-grid. The model has a fully elastic non-hydrostatic option (Yeh et al. 2002), in which case the vertical coordinate is the terrain-following hydrostatic pressure (Laprise 1992). In CRCM5, a sponge zone (Davies 1976) of ten grid points is applied around the perimeter of the regional domain where the inner solution is gradually blended with the outer solution imposed as LBC.

The model configuration uses Kain-Fritsch deep convection parameterization (Kain and Fritsch 1990), Kuo-transient shallow convection (Kuo 1965; Bélair et al. 2005), Sundqvist resolved-scale condensation (Sundqvist et al. 1989), correlated-K terrestrial and solar radiation schemes (Li and Barker 2005), subgrid-scale orographic effects are parameterized following the McFarlane mountain

gravity-wave drag (McFarlane 1987) and the low-level orographic blocking scheme of (Zadra et al. 2003), and turbulent kinetic energy closure planetary boundary layer and vertical diffusion (Benoit et al. 1989; Delage and Girard 1992; Delage 1997). Unlike the NWP version of GEM, however, CRCM5 uses the most recent version of the Canadian Land Surface Scheme (CLASS 3.5; Verseghy 2000, 2008) that allows for a detailed representation of vegetation, land-surface types, organic soil and a flexible number of layers.

3 Experimental design

Regional climate model simulations resulting from single- and double-nesting approaches are compared using the Big-Brother Experiment (BBE) protocol as devised originally by Denis et al. (2002b). This experiment is a perfect prognosis approach that isolates the nesting errors from other modelling errors, thus emphasizing the influence of nesting on the RCM solution.

In the BBE, a first simulation using the desired grid mesh is realized on a very large domain. This simulation, named the Big Brother (BB), serves two purposes: (1) it is used as reference to evaluate the test simulations nicknamed the Little-Brother (LB) simulations, and (2) it provides, after filtering manipulations described below, IC and LBC to LB simulations. In our case, we used as Big Brother a CRCM5 simulation on a 0.15° mesh covering a 760 × 760 gridpoint domain centred on Montréal, Québec, Canada, with 56 levels in the vertical. The Big-Brother simulations were driven by ERA-Interim reanalysis for four two-month periods starting November first of the years 1997, 1998, 1999 and 2000 (see Fig. 1 for experimental design and Fig. 2 for domains location and size). These Big-Brother simulations will be noted BB.15.

In an attempt to mimic the case when a low-resolution GCM simulation provides IC and LBC for dynamical downscaling, the BB-simulated data is processes by a low-pass filter that retains only the large scales; the resulting dataset is termed "filtered BB" (BB.15_Fr), with "r" the equivalent mesh size resolution. These BB.15_Fr fields are in some sense perfect as far as the large-scale fields are concerned, because they do not suffer from simulation errors that would occur in coarse-mesh model simulations. Diaconescu et al. (2007) mentioned that those are due to the inability to represent fine-scale topography and the eddy processes, the imperfection in capturing internal variability and difficulty in parameterizing subgrid-scale processes. BB.15_Fr fields are devoid, however, of small scales, as do coarse-mesh GCM simulations. The BB.15_Fr dataset is used as IC and LBC for LB simulations that are performed using the same model formulation and resolution as the BB.15, but driven by BB.15_Fr data over smaller domains. These LB simulations are evaluated by comparing with the reference BB simulation. The differences between the LB and BB.15 can be unambiguously attributed to nesting errors because of such perfect-prognosis protocol.

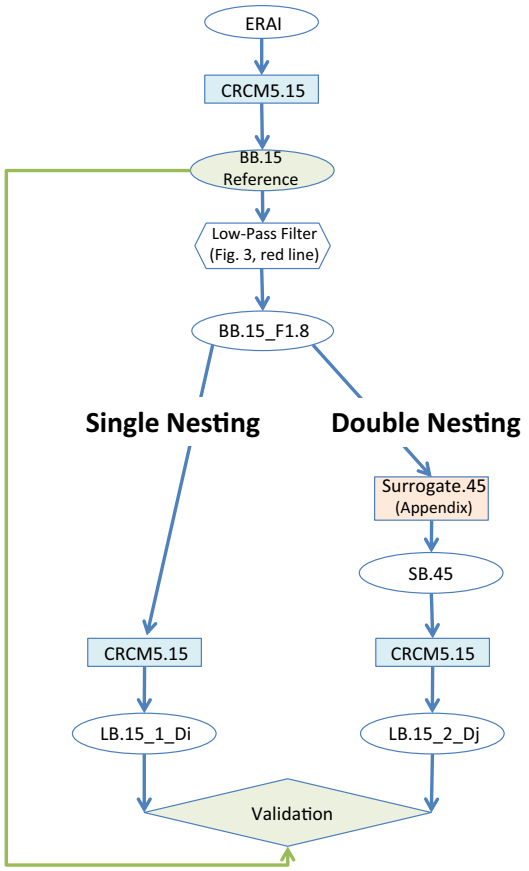

Fig. 1 The experimental flowchart. Era-interim (ERAI) is used to drive the CRCM5 on a 0.15° mesh (RCM.15), the result is the Big-Brother simulation (BB.15). This simulation is used as reference to validate the Little-Brother (LB) simulation and also processed by a low-pass filter creating BB.15_F1.8, which is used as driving data for the two approaches. For the single nesting, the BB.15_F1.8 dataset is used to drive the CRCM5 on a 0.15° mesh (CRCM5.15) on multiple domain size (Di) with the same configuration used to simulate BB.15. The resulting datasets [LB.15_1_Di: Little-Brother simulations for the i domain sizes of the single nesting (see Fig. 2)] are compared to BB.15. For the double nesting, the BB.15_F1.8 dataset is used to create the surrogate intermediate simulation (Surrogate.45: see "Appendix") that provides the SB.45 dataset used to drive the CRCM5 on a 0.15° mesh (CRCM5.15) on multiple domain size (Dj) with the same configuration used to simulate BB.15 [LB.15_2_Dj: Little-Brother simulations for the j domain sizes of the double nesting (see Fig. 2)] are compared to BB.15 and LB.15_1_Di

The low-pass filter is based on the discrete cosine transform (Denis et al. 2002a), with a gradual response function that attempts to mimic the spectrum of an equivalent 1.8°-mesh simulation. The lower and upper wavelength

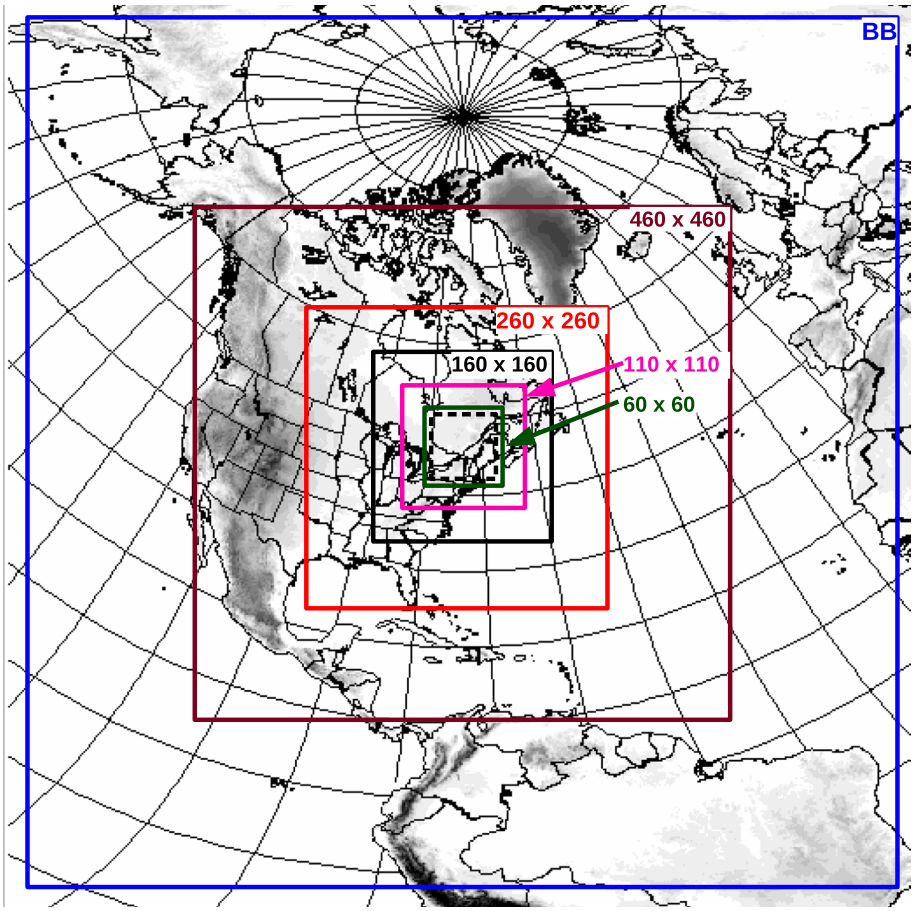

Fig. 2 The simulation domains for the BB.15 (760 × 760 grid points), the LBs with domain size of 460 × 460, 260 × 260, 160 × 160, 110 × 110 and 60 × 60 grid points for the single nesting (Fig. 1: LB.15_1_Di) and 260 × 260, 160 × 160, 110 × 110 and 60 × 60 grid points for the double nesting (Fig. 1: LB.15_2_Dj). Climate statistics were computed in the *black dashed square area* of 44 × 44 grid points

limits for the BB.15_F1.8 are chosen to be 396 and 1386 km, corresponding respectively to the Nyquist length scale 2 Δx and to the smallest adequately resolved scales 7 Δx, as shown by Skamarock (2004) and Cholette et al. (2015); a cosine-squared function response is used between these two limits (as shown by the red line in Fig. 3).

Two dynamical downscaling approaches will be compared using the BBE protocol: the single and double nesting, as shown on Fig. 1.

3.1 Single-nesting approach

The LB simulations using the single nesting follow the usual BBE protocol as in (Denis et al. 2002b). In our case, the LB simulations were performed for four 1.5-month periods starting on November 15 (thus leaving out the initial 15 days as spin-up of the BB.15 simulations), for the years 1997–2000, using the BBF dataset as IC and LBC at 6 h intervals. The LB simulations were performed over five different domain sizes: 460 × 460, 260 × 260, 160 × 160, 110 × 110 and 60 × 60 grid points, respectively (Fig. 2). The climate statistics of the LB were compared to those of the BB for the 4 months

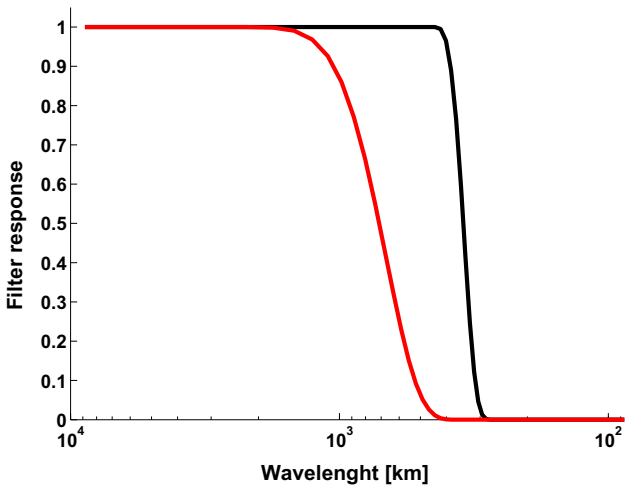

Fig. 3 Filter response for the BB filter (*red line*) and the analysis filter (*black line*)

of December (thus leaving out the initial 15 days as spin-up of the LB simulations) over a common area of 44 × 44 grid points indicated by the dashed black square in Fig. 2.

3.2 Double-nesting approach

While the single nesting follows the standard BBE procedure, the design of the double-nesting experiment deserves special attention. The challenge is to maintain the perfect-prognosis attribute of the BBE while designing a double-nesting strategy that normally involves the use of an intermediate-resolution simulation. After considering several alternatives, the following procedure was adopted. A surrogate to an intermediate-resolution simulation on a 0.45° mesh has been generated using a 0.15°-mesh simulation performed over a moderately large domain, and then using specific filters to replicate the spectral characteristics and behaviour of a 0.45°-mesh simulation over an optimal domain size. The resulting simulation data will be referred to as Step Brother (SB.45). The "Appendix" details the procedure followed to determine the optimal conditions so that the SB.45 dataset represents a good proxy to an idealized 0.45°-mesh simulation while maintaining the perfect-prognosis approach using 0.15°-mesh LB simulations.

The SB.45 dataset corresponds to the first stage of the double-nesting procedure in Fig. 1. In turn, this SB.45 dataset serves to drive a 0.15°-mesh LB simulations for the second stage of double nesting. Several 0.15°-mesh LB simulations were performed on various domain sizes (260×260, 160×160, 110×110 and 60×60 grid points, respectively), using a nesting interval of 1 h.

4 Analysis tools

A proper evaluation of high-resolution nested RCM simulations requires separating the large scales that are present in the driving LBC from the smaller scales that are only resolved by the finer mesh of the RCM. The black line in Fig. 3 shows the response of the analysis filter used to isolate the large-scale component: wavelengths longer than 400 km are retained entirely and those smaller than 300 km are removed, with a gradual cosine-squared function transition in between. The small-scale component is obtained by subtracting the large-scale component from the original fields. In particular, large scales refer to those scales present in the driving data and small scales correspond to those absent in the driving data. It is important to note that the analysis filter has been applied on a common area for all simulations, irrespective of the simulation domains.

Temporal decomposition of each variables Ψ is applied before analysis. Any variable $(\Psi(\mathbf{x},t))$ function of space $\mathbf{x}$ and time t will be split to analyze their time mean (also called stationary component) and time deviation (also called transient-eddy component), as follows

$$\Psi(\mathbf{x},t) = \overline{\Psi}(\mathbf{x}) + \Psi'(\mathbf{x},t) \tag{1}$$

where $\bar{\bullet}$ is the temporal mean and ' the time deviation. The transient-eddy variance is obtained as

$$\sigma'^2(\mathbf{x}) = \overline{\Psi'^2}(\mathbf{x}) \tag{2}$$

The LB and BB statistics will be compared in terms of the ratio of their transient-eddy standard deviation (SD)

$$\Gamma' = \frac{\sigma'_{LB}(\mathbf{x})}{\sigma'_{BB}(\mathbf{x})}, \tag{3}$$

the transient-eddy correlation

$$\rho'(\mathbf{x}) = \frac{\overline{\left(\Psi'_{BB}(\mathbf{x},t) * \Psi'_{LB}(\mathbf{x},t)\right)}}{\sigma'_{BB}(\mathbf{x})\sigma'_{LB}(\mathbf{x})}, \tag{4}$$

and the transient-eddy root mean square (RMS) difference

$$RMS'(\mathbf{x}) = \sqrt{\overline{\left(\Psi'_{LB}(\mathbf{x},t) - \Psi'_{BB}(\mathbf{x},t)\right)^2}}. \tag{5}$$

Likewise, statistics from spatial structure will be obtained as follows

$$\overline{\Psi}(\mathbf{x}) = \langle\overline{\Psi}(\mathbf{x})\rangle + \Psi^*(\mathbf{x}), \tag{6}$$

where $\langle\rangle$ and * refer, respectively, to the spatial average and the spatial deviation of the field; the spatial-eddy variance is defined as

$$\sigma^{*2} = \langle\Psi^{*2}(\mathbf{x})\rangle. \tag{7}$$

The LB and BB statistics can be compared in terms of the ratio of spatial SD as

$$\Gamma^* = \frac{\sigma^*_{LB}}{\sigma^*_{BB}}, \tag{8}$$

the spatial correlation as

$$\rho^* = \frac{\langle\Psi^*_{BB}(\mathbf{x})\Psi^*_{LB}(\mathbf{x})\rangle}{\sigma^*_{BB}\sigma^*_{LB}}, \tag{9}$$

and the RMS difference of spatial deviation as

$$RMS^* = \sqrt{\left\langle\left(\Psi^*_{LB}(\mathbf{x}) - \Psi^*_{BB}(\mathbf{x})\right)^2\right\rangle}. \tag{10}$$

The Taylor diagrams (Taylor 2001) are useful to summarise succinctly the spatial and temporal behaviours of the LBs compared to the BB.15_F1.8. On the presented diagrams, the RMS are normalized by the SD of the BB.

5 Results

In this section, selected variables are presented to give a representative picture of the general behaviour of the spatial and temporal properties.

5.1 Stationary component

The large-scale stationary component of the simulations has been investigated. Figure 4 shows the Taylor diagrams for the large-scale stationary component of both the single- and double-nesting LB simulations over various domain sizes. They were compared to the reference BB.15, for the mean sea level pressure (Fig. 4a) and the 850-hPa relative humidity (Fig. 4b) fields.

These two variables have their spatial structure dominated by large-scale stationary component. Given that the large scales are driven by the LBC, all LB simulations showed a rather high skill level, except for the largest domain sizes that show weaker spatial correlations and larger amplitude errors, which confirmed earlier results about the influence of RCM domain sizes. The mean sea level pressure field is particularly well reproduced, as also noted by Leduc and Laprise (2009), except for the largest domain with both approaches. A glance at 2-D large-scale map (not shown) confirmed that, for all cases, there are quite similar, and small differences are not physically meaningful. There is overall little difference between the single- and double-nesting results, although we noted that over the smallest domains the best correlation with the double nesting is slightly lower than that with the single nesting.

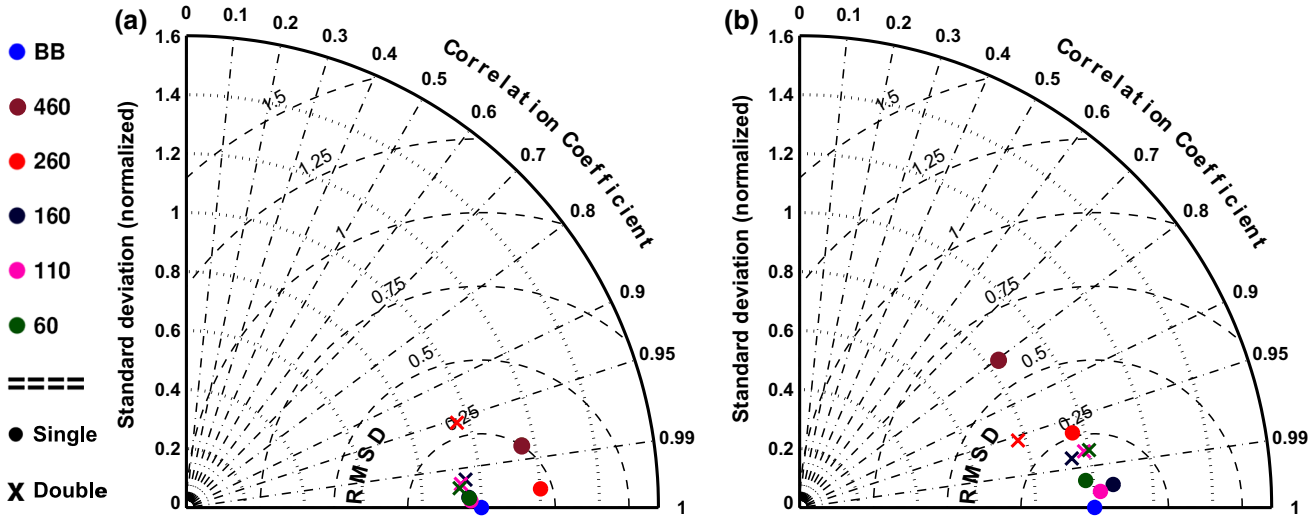

Fig. 4 Large-scale stationary component of the mean sea level pressure (**a**) and 850-hPa relative humidity (**b**) fields. The *dots* correspond to the single-nesting results and the crosses to the double-nesting results. The *colours* correspond to the various domain sizes of the LB. The *blue dot* corresponds to the reference BB.15 simulation

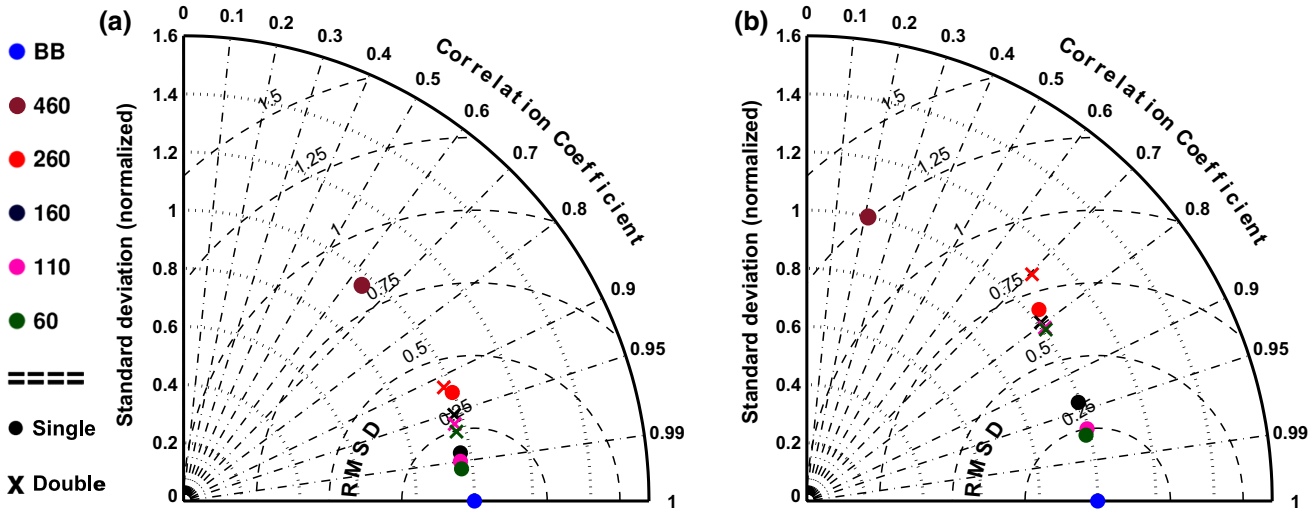

Fig. 5 Spatial mean of the large-scale transient-eddy component of 300-hPa meridional wind (**a**) and 850-hPa relative humidity (**b**)

The amplitude of the small-scale stationary component is negligible compared to that of the large scales, and hence results are not shown.

5.2 Transient-eddy component

In this section, the transient-eddy component is examined. The transient-eddy component represents the day-to-day meteorological fluctuations. Figure 5 presents the spatial mean of the large-scale transient-eddy statistics for 300-hPa meridional wind component (Fig. 5a) and 850-hPa relative humidity (Fig. 5b). These results illustrate that large-scale transient-eddy amplitudes are well represented, independently of domain size and the use of single or double nesting. The time correlation, however, decreases with increasing domain size, reflecting the weaker control exerted by LBC with larger domains, and this is somewhat more pronounced with double nesting.

Figure 6 presents the small-scale transient-eddy component of 700-hPa relative vorticity (Fig. 6a) and 850-hPa relative humidity (Fig. 6b). These variables have been selected because the spectral slope of their variance spectra is much flatter, reflecting the fact that their spatial structure contains substantial small-scale features. As mentioned by Leduc and Laprise (2009), small-scale features are fluctuations, absent from the LBC, causes by the interaction from large flow with local fine-scale forcing (such as topography, the land-surface heterogeneities and other subgrid-scale parameterized physical processes). The most notable feature shown in Fig. 6 is that the time correlation is very weak, which is to be expected given that LBC do not contain small-scale informations. The remaining, non-vanishing time correlation is probably due a second-order effect of preconditioning of small-scale features by the time-fluctuating large-scale flow interacting with fine-scale surface forcing. For large domains the amplitude of small-scale transient-eddy converges to the correct value (a value of one in relative terms). For single-nesting simulations over smaller domains, however, the small-scale transient eddies are amplitude-deficient, reflecting the fact that the complete spin-up of small scales did not have enough room to occur. This effect is not as clear in Fig. 6b mainly because at 850-hPa surface forcing effect is still noticeable which promotes the development of small-scale features. This has also been noted, in a more pronounced way, over the Canadian Rocky Mountains (Antic et al. 2004). Double-nesting simulations, on the other hand, hardly suffer from such spin-up problem because of the smaller resolution jump afforded by the use of the first step in the cascade with the surrogate intermediate-resolution SB.45. Therefore, only the simulation performed on the smallest 60 × 60 grid-point domain shows some amplitude deficiency.

These results highlight important differences between the single- and double-nesting results. As the domain size is reduced, the results from single nesting showed a clear underestimation of the small-scale transient-eddy amplitude, which was referred to by Leduc and Laprise (2009) as the spatial spin-up issue. This occurs when a domain is too small to allow the full development of the small scales for a given resolution jump between the driving LBC and the RCM grid mesh. Double nesting clearly leads to a reduction of the spatial spin-up issue due to the use of the intermediate-resolution simulation (SB.45). For this case, the double nesting allows to halve the domain size of the high-resolution simulation, which implies a clear reduction in computational cost.

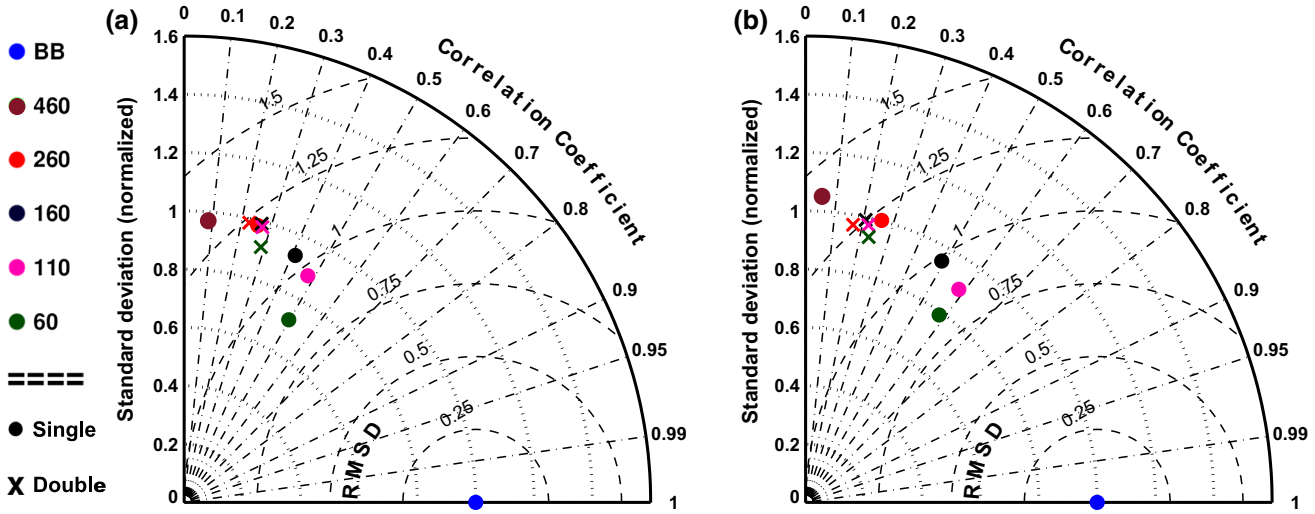

Fig. 6 Small-scale transient-eddy component of 700-hPa relative vorticity (**a**) and 850-hPa relative humidity (**b**)

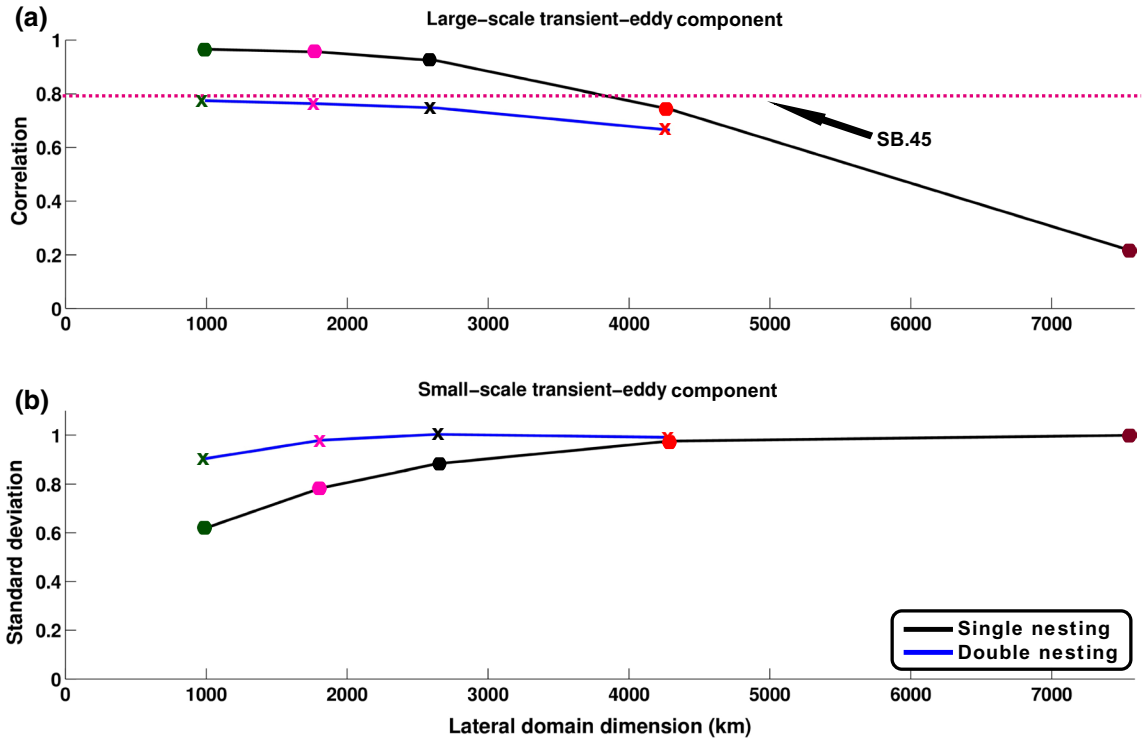

Fig. 7 Transient-eddy statistics for the single nesting (*solid black line*) and the double nesting (*solid blue line*). The first figure **a** represents the large-scale transient-eddy correlation and the second figure **b** the small-scale transient-eddy SD for the relative humidity at 700 hPa by the lateral domain dimension (km). The magenta *dashed line* represents the large-scale transient-eddy correlation of the SB.45 simulation

5.3 Single nesting Versus double nesting

The previous results can succinctly be summarised by looking at Fig. 7, which shows the 700-hPa relative humidity field statistics as a function of the horizontal domain dimension in abscissa. The choice of introducing another variable that has not been shown yet in this study was made to show that the general behaviour is common to many variables. Figure 7a shows the time correlation of large-scale transient eddies and Fig. 7b the relative small-scale transient-eddy SD. The black and blue lines correspond to the statistics of the single- and the double-nesting simulations, respectively. An increase of the large-scale transient-eddy time correlation is noted as the domain size decreases, asymptoting to unity for single-nesting approach and to about 0.8 for double-nesting approach. The somewhat less than unity asymptotic value for double nesting arises from the use of a surrogate intermediate-resolution simulation, which introduced an upper bound to the skill of the ensuing LB in the second step with the double-nesting approach (see "Appendix").

The small-scale transient-eddy SD (Fig. 7b) clearly shows the effect of spatial spin-up. The single nesting shows a marked decrease of the SD for a smaller lateral domain dimension of 260 grid points (≈ 4300 km). Whereas with double nesting the domain dimension can be reduced to as small as 110 grid points (≈1800 km) before a marked amplitude deficiency occurs. The sensitivity of the small scales is much reduced with the double-nesting approach, because the smaller resolution jump between each step in the cascade results in a reduced spatial spin-up requirement. The main conclusion from the single-nesting results is that with domains larger than about 2600 km the control exerted by the LBC is too weak and that domains smaller than about 4300 km do not allow sufficient spin-up space.

As also noted in Fig. 7a, the double-nesting results, however, showed that the large scales suffer from some lack of time correlation, even for small domain sizes. This is due to some loss of correlation in the first step (i.e. SB.45, see "Appendix") in the double-nesting approach. The issue of the less than unity time correlation of large scales with double nesting can be addressed through the application of large-scale spectral nudging (e.g. Von Storch et al. 2000) in generating the LB. Figure 8 shows results that are equivalent to those previously shown in Fig. 7, but obtained with spectral nudging activated in generating the surrogate intermediate-resolution simulation needed in the double-nesting approach. Figure 8a shows that double-nesting results with spectral nudging become rather similar to those of single nesting. Indeed, it

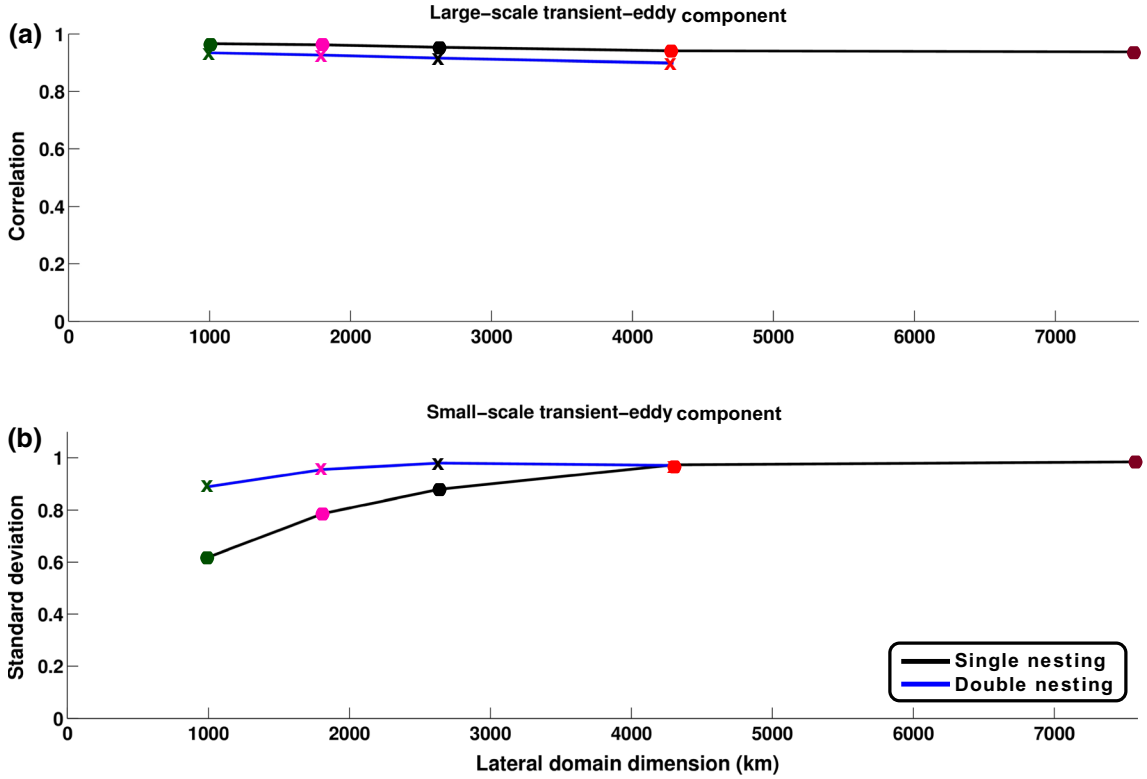

Fig. 8 Same as Fig. 7 but with large-scale spectral nudging activated in generating the LBs. The SN was applied to horizontal wind components with horizontal length scales larger than 1000 km, with a recall strength set to zero below the 850-hPa level, then increasing linearly to its maximum value at 500 hPa, and remaining constant to the model top level. The spectral nudging maximum strength is 1.3% applied at each time step

shows little sensitivity of large-scale transient-eddy time correlation with domain size, and the asymptotic value for double-nesting strategy approaches unity for small domains. Small-scale transient-eddy statistics (Fig. 8b) show hardly any sensitivity to the application of spectral nudging, for both single- and double-nesting approaches, which makes sense given that spectral nudging by definition only affects the large scales.

6 Summary and discussions

The resolution jump between a nested RCM and its driving data is an important parameter in dynamical downscaling applications. For large jumps, spatial spin-up must be taken in consideration when choosing an RCM domain size to allow an adequate development of small scales within the limited-area domain. Multiple dynamical downscaling might offer beneficial perspectives to achieve high-resolution regional climate simulations, although its use may have an impact on the simulations quality. The objective of this work was to investigate the impact of multiple dynamical downscaling by comparing single- and double-nesting approaches for climate simulations within the Big-Brother Experimental protocol.

A Big-Brother simulation was performed with CRCM5 on a 0.15° mesh over a very large domain for four periods of two winter months. This BB.15 simulation was then filtered to an equivalent 1.8°-mesh typical of operational global climate models. The resulting dataset (noted BB.15_F1.8) was used to drive a series of 0.15°-mesh Little Brother (LB) simulations in the single-nesting case. In the double-nesting case, an additional simulation (nicknamed Step Brother, SB.45) was introduced as a surrogate to an intermediate-resolution (0.45° mesh) model to drive the LB (as described in "Appendix").

The study of the time-averaged (stationary) component, which is dominated by large scales, has not shown much difference between the two approaches. In both cases, the use of excessively large domains (greater than 260 × 260 grid points in our application) resulted in a lack of control exerted by the LBC.

Transient-eddy component shows more sensitivity to varying domain size. The double-nesting approach exhibits a small but systematic reduction in time correlation compared to the single-nesting approach. The culprit is the intermediary simulation that introduces a weakening of control by the LBC. From a climate-simulation point of view, temporal correlation is generally not of paramount importance. If,

however, a specific application required improved temporal correlation, such as for case studies, then large-scale spectral nudging could be used advantageously.

The largest sensitivity to domain size was noted in the small-scale transient eddies. With single nesting, small domain sizes (smaller than 260 × 260 grid points in our application) resulted in amplitude-deficient small-scale transient eddies due to insufficient spatial spin-up. This effect is greatly reduced with double nesting, and adequate amplitudes are recovered with much smaller domains (as small as 110 × 110 grid points in our application). These results were traced back to the use of the intermediate-resolution simulation in the double nesting approach, which reduces the effective resolution jump, drastically decreases the effect of spatial spin-up, and allows a reduction of the optimal domain size of the high-resolution simulation, resulting in important computational savings.

In summary, the results obtained within the BBE protocol indicated that a minimum lateral domain dimension of about 4300 km was required when driving a 0.15°-mesh RCM with 1.8°-mesh LBC to ensure an adequate development of the small-scale features with single nesting, while with double nesting, this minimum lateral domain size is reduced to about 1800 km. This reduction of the minimum required domain size leads to reduce the computational cost (including the small computational cost of the intermediate-resolution simulation) by nearly a factor of 5. This represents an important gain in term of computing resources required to perform high-resolution climate simulations.

Acknowledgments This research was supported by the Natural Sciences and Engineering Research Council (NSERC) of Canada. Computations were made on the supercomputer guillimin, managed by *Calcul Québec* and Compute Canada. The operation of this supercomputer is funded by the Canada Foundation for Innovation (CFI), the *Fonds de recherche du Québec—Nature et technologies* (FRQ-NT), NanoQuébec, and the *Réseau de médecine génétique appliquée* (RMGA). The authors are greatly indebted to Dr. Bernard Dugas and Ms. Katja Winger for their essential help with the use of CRCM5, and to Mr. Georges Huard and Ms. Nadjet Labassi for maintaining user-friendly local computing facilities.

Appendix

The double-nesting approach requires the introduction of an intermediate-resolution simulation between the 1.8° coarse-mesh driving LBC and the final 0.15° fine-mesh RCM simulations (Fig. 1: double nesting). This additional simulation (named Step Brother, SB.45) needs to be carefully designed to satisfy two criteria: (1) to generate a dataset with characteristics similar to those of a 0.45°-mesh simulation, but (2) to use the same 0.15°-mesh RCM to maintain the perfect-prognosis nature of the BBE protocol. To satisfy these requirements, a surrogate to an intermediate-resolution (0.45° mesh) simulation was generated using a 0.15°-mesh RCM simulation performed and massaged under specific conditions as shown in Fig. 9 and described below into three steps. The first step (step A) aims at finding the optimal domain size for the intermediate-resolution and highlighting its statistics needed for the next step. The second step (step B) is important for finding the optimal spectral nudging configuration for a 0.15°-mesh simulation that will fit better the statistics of the optimal domain size found in step A. Finally, step C has been designed to find the appropriate filter that fits the variance spectrum of a 0.45°-mesh simulation.

Step A: the optimum domain for the intermediate-resolution simulation

We address these requirements by performing another set of BBE with a 0.45°-mesh RCM with single nesting. In this case, the BB.45 simulation covers a large, 260 × 260 grid-point domain (not shown) centred on Montréal, Québec, Canada, with a 0.45° mesh. As before the BB.45 simulations were driven by Era-Interim reanalysis for four two-month periods starting on November first of the years 1997, 1998, 1999 and 2000. The same low-pass filter as described in Sect. 3 is applied on BB.45 (reproduced for convenience as the red line in Fig. 10) to serve as IC and LBC for subsequent LB simulations (LB.45). The LB.45 simulations were performed for four 1.5-month periods starting on November 15th for years 1997, 1998, 1999 and 2000, using BB.45_F1.8 at 6 h intervals. Five simulations were performed over different domain sizes of 180 × 180, 120 × 120, 90 × 90, 70 × 70 and 50 × 50 grid points, respectively (domains not shown). The climate statistics were computed on a common area of 38 × 38 grid points centred over Montréal, Québec, Canada, for the 4 months of December. For analysis the large and small scales are separated using a low-pass filter shown by the black line in Fig. 10.

Only a small sample of the results obtained from this BBE will be discussed to identify the optimum domain size. Figure 11a shows the Taylor diagram of the time-averaged, stationary component of the relative humidity field at 850 hPa. The smaller domain simulations (90 × 90, 70 × 70 and 50 × 50 grid points) exhibit excellent spatial correlation and amplitude, while the larger domains (180 × 180

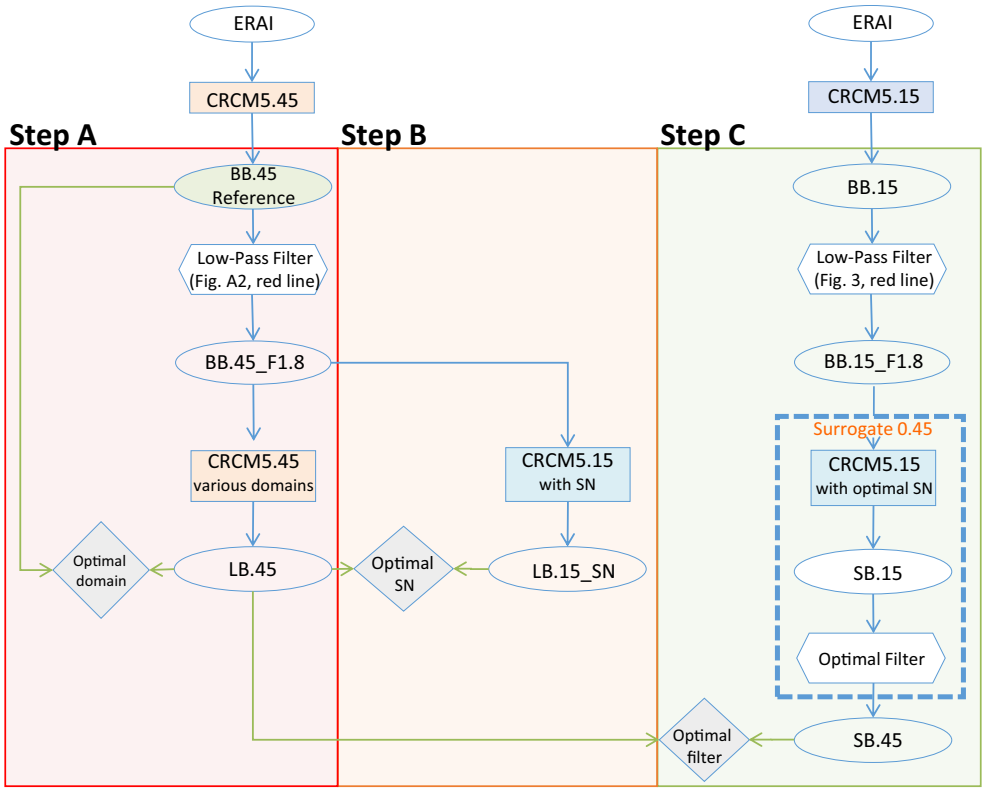

Fig. 9 Flowchart of the protocol for the surrogate simulation. For the *step A*, Era-Interim (ERAI) is used to drive the CRCM5 at 0.45° mesh (CRCM5.45), the result is the Big-Brother simulation (BB.45). This simulation is used as reference to validate the Little-Brother (LB.45) simulation and also processed by a low-pass filter creating BB.45_F1.8 that is used as driving data for the CRCM5 (CRCM5.45; various domains) on various domain sizes with the same configuration used to simulate BB.45. The resulting datasets (LB.45) are compared to BB.45 to highlight the optimal domain size. For the *step B*, BB.45_F1.8 is used to drive the CRCM5 (CRCM5.45; with SN) on a unique domain size with different spectral nudging configurations. The large scales of the resulting datasets (LB.15_SN) are compared with optimal domain size simulation from the previous step. For the *step C*, Era-Interim (ERAI) is used to drive the CRCM5 at 0.15°-mesh (CRCM5.15), the result is the Big-Brother simulation (BB.15: same as in Sect. 3). This simulation is processed by a low-pass filter creating BB.15_F1.8 (same as in Sect. 3) which is used as driving data for the CRCM5 at 0.15°-mesh with the optimal spectral nudging configuration highlights in step B (CRCM5.15; with optimal SN). The resulting dataset (SB.15) has been processed by several spectral filters and results compared to the variance spectrum of LB.45 in order to find the optimal spectral filter. The results dataset is the surrogate simulation (SB.45) as presented in Fig. 1

and 120 × 120 grid points) exhibit weaker spatial correlations, indicating a weaker control exerted by the LBC. Figure 11b shows the Taylor diagram of the small-scale transient-eddy component of the relative humidity field at 700 hPa. It shows a gradual decrease of time correlation as the domain size increases, indicative of the lesser control exerted by the LBC, but a small deficit of amplitude as the domain is reduced, reflecting the aforementioned spatial spin-up issue. Overall, the 90 × 90 grid-point domain appears to offer the best compromise, being large enough to allow the full development of the small scales permitted by the grid mesh, but not too large so as to maintain suitable control by the LBC driving data. For these reasons this domain size has been chosen as the optimal domain size.

This 0.45°-mesh simulation however cannot be used as the first step of the double nesting because it would contravene the perfect-prognosis nature of the BBE approach. To avoid this pitfall, a 0.15°-mesh RCM must be used that emulates the characteristics of a 0.45°-mesh simulation. This 0.45°-mesh simulation over the optimal domain will be used as reference to: (1) find the optimal spectral nudging configuration that one must apply on a 0.15°-mesh RCM simulation to correctly reproduce the large-scale of a 0.45°-mesh simulation (as detailed in step B), and to (2) find the optimal filter that one must apply on a 0.15°-mesh RCM simulation to correctly reproduce the small scales of a 0.45°-mesh simulation (as detailed in step C).

Step B: the optimum large-scale spectral nudging

The BB.45_F1.8 dataset was used to drive a 460 × 460 grid-point simulation (Fig. 2 same as the burgundy domain)

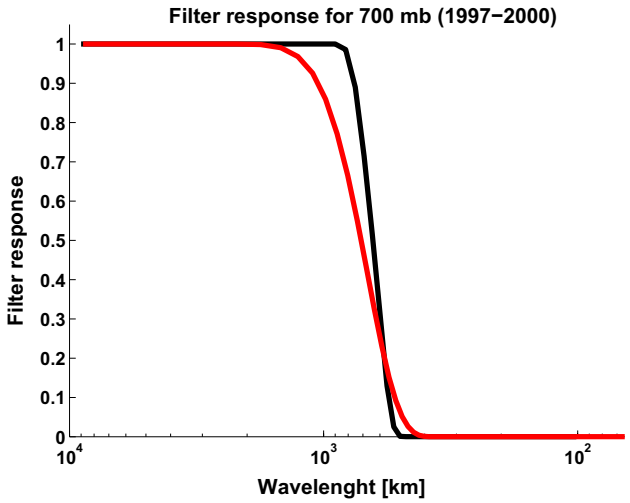

Fig. 10 Filter response for the BB filter (red line) and the analysis filter (black line)

on a 0.15° mesh with spectral nudging (SN) activated (Fig. 9: CRCM5.15 with SN). A large domain was used to ensure the full development of the small scales and spectral nudging was applied to control the large scales. The nudging parameters were tuned to reproduce the large-scale statistics of the LB.45. After several tests it has been found that nudging the horizontal wind for wavelengths larger than 1000 km, with strength set to zero below the 600-hPa level and increasing linearly with height until the top model level, with a maximum strength of 1.4% applied at each time step. This configuration is used as optimal spectral nudging configuration in step C.

Step C: Optimal filter to reproduce the variance spectrum of a 0.45°-mesh simulation

Another simulation of the 0.15°-mesh simulation over a 460 × 460 grid-point domain (Fig. 9: CRCM5.15 with optimal SN), driven by the original BB.15_F1.8 data at 6 h intervals (same as Sect. 3) was performed with the optimal SN parameters found in step B. The corresponding dataset (Fig. 9: SB.15) has then a large-scale behaviour of LB.45 over the optimal domain, but an incorrect small-scale behaviour. To adjust that, a specific low-pass filter was then designed in such a way that the variance spectrum of this 0.15°-mesh simulation best approximates the reference 0.45°-mesh simulation. Figure 12 shows the energy spectrum for the 700-200 hPa atmospheric layer of the reference 0.45°-mesh simulation driven by BB.45_F1.8 (LB.45; red line), 0.15°-mesh simulation with optimal SN parameters driven by BB.15_F1.8 (SB.15; black line), and the resulting optimally filtered version of the latter (SB.45; blue line). To correctly simulate a 0.15°-mesh simulation that has properties of a 0.45°-mesh simulation, a filter should have been used that cuts the tail of SB.45 represented by the dashed blue line in Fig. 12. But for the experiment shown, this was not done; a parallel experiment has shown that it has almost no influence on the results presented in this study. This dataset will be used as driving data for the second step of the double-nesting simulations.

In summary, the SB.45 dataset represents in some sense perfect LBC as required by the BBE protocol, in the sense that it is produced by the same model at the same resolution and, compared to an equivalent 0.45°-mesh simulation,

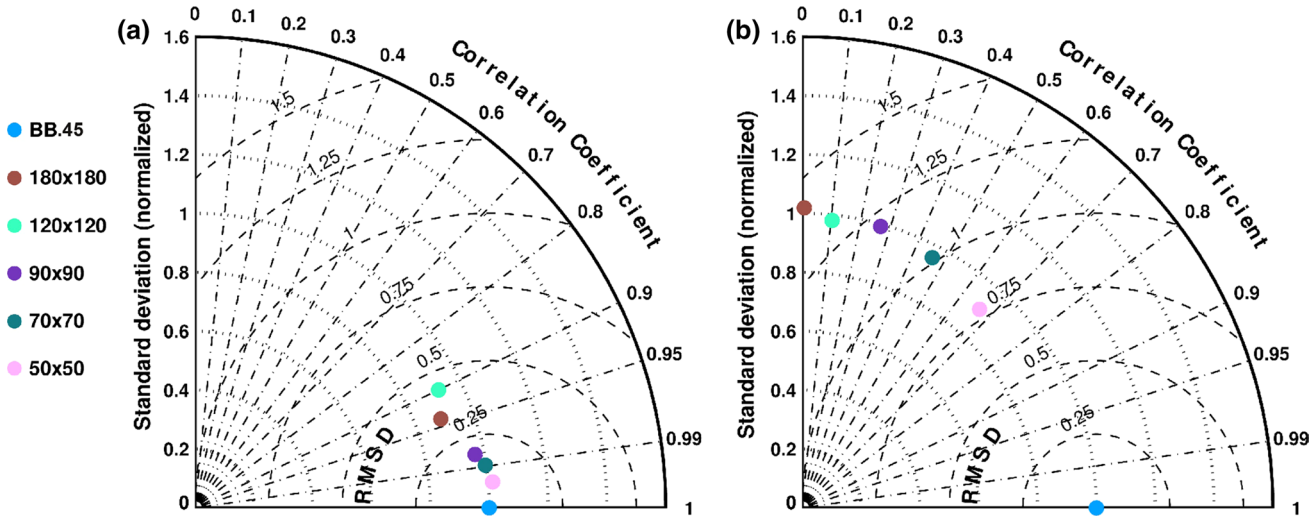

Fig. 11 Relative humidity statistics from the Big-Brother experiment realized at 0.45° mesh for the stationary component of the original fields at 850 hPa (a) and the transient-eddy component of the small-scale field at 700 hPa (b)

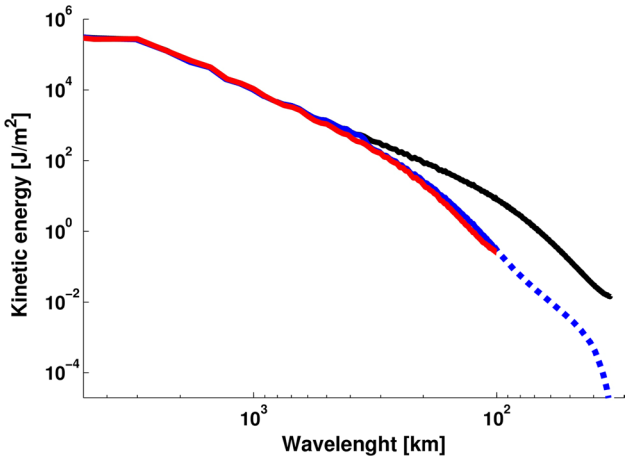

Fig. 12 Kinetic energy spectrum for the 700–200 hPa atmospheric layer, averaged for 1997, 1998, 1999 and 2000, for the various simulations. The *red line* corresponds to 0.45°-mesh simulation driven by BB.45_F1.8 (noted LB.45 in Fig. 9), the *black line* to the 0.15°-mesh simulation with optimal SN parameters driven by BB.15_F1.8 (noted SB.15 in the Fig. 9), and the *blue line* the optimally filtered version of the latter (noted SB.45 in the Fig. 9)

it has a similar skill as discussed in step B above and similar variance spectrum as discussed in step C above.

References

Antic S, Laprise R, Denis B, de Elía R (2004) Testing the downscaling ability of a one-way nested regional climate model in regions of complex topography. Clim Dyn 23(5):473–493. doi:10.1007/s00382-004-0438-5

Ban N, Schmidli J, Schär C (2015) Heavy precipitation in a changing climate: Does shortterm summer precipitation increase faster? Geophys Res Lett 42(4):1165–1172. doi:10.1002/2014GL062588

Bélair S, Mailhot J, Girard C, Vaillancourt P (2005) Boundary layer and shallow cumulus clouds in a medium-range forecast of a large-scale weather system. Mon Weather Rev 133(7):1938–1960

Benoit R, Côté J, Mailhot J (1989) Inclusion of a TKE boundary layer parameterization in the Canadian regional finite-element model. Mon Weather Rev 117(8):1726–1750

Brisson E, Demuzere M, van Lipzig NP (2015) Modelling strategies for performing convection-permitting climate simulations. Meteorol Z. doi:10.1127/metz/2015/0598

Chan S, Kendon E, Fowler H, Blenkinsop S, Ferro CT, Stephenson D (2012) Does increasing the spatial resolution of a regional climate model improve the simulated daily precipitation? Clim Dyn 1–21. doi:10.1007/s00382-012-1568-9

Cholette M, Laprise R, Thériault JM (2015) Perspectives for very high-resolution climate simulations with nested models: Illustration of potential in simulating St. Lawrence River valley channelling winds with the fifth-generation Canadian Regional Climate Model. Climate 3(2):283–307. doi:10.3390/cli3020283

Côté J, Desmarais JG, Gravel S, Méthot A, Patoine A, Roch M, Staniforth A (1998a) The operational CMC-MRB global environmental multiscale (GEM) model. Part II: results. Mon Weather Rev 126(6):1397–1418

Côté J, Gravel S, Méthot A, Patoine A, Roch M, Staniforth A (1998b) The operational CMC-MRB global environmental multiscale (GEM) model. Part I: design considerations and formulation. Mon Weather Rev 126(6):1373–1395

Davies H (1976) A lateral boundary formulation for multilevel prediction models. Q J Roy Meteorol Soc 102(432):405–418

Delage Y, Girard C (1992) Stability functions correct at the free convection limit and consistent for both the surface and Ekman layers. Bound Layer Meteorol 58(1–2):19–31

Delage YAA (1997) Parameterising sub-grid scale vertical transport in atmospheric models under statically stable conditions. Bound Layer Meteorol 82(1):23–48

Denis B, Côté J, Laprise R (2002) Spectral decomposition of two-dimensional atmospheric fields on limited-area domains using the discrete cosine transform (DCT). Mon Weather Rev 130(7):1812–1829

Denis B, Laprise R, Caya D, Côté J (2002b) Downscaling ability of one-way nested regional climate models: the Big-Brother Experiment. Clim Dyn 18(8):627–646. doi:10.1007/s00382-001-0201-0

Di Luca A, de Elía R, Laprise R (2015) Challenges in the quest for added value of regional climate dynamical downscaling. Curr Clim Change Rep 1(1):10–21. doi:10.1007/s40641-015-0003-9

Diaconescu EP, Laprise R, Sushama L (2007) The impact of lateral boundary data errors on the simulated climate of a nested regional climate model. Clim Dyn 28(4):335–350. doi:10.1007/s00382-006-0189-6

Hernández-Díaz L, Laprise R, Sushama L, Martynov A, Winger K, Dugas B (2013) Climate simulation over CORDEX Africa domain using the fifth-generation Canadian Regional Climate Model (CRCM5). Clim Dyn 40(5–6):1415–1433. doi:10.1007/s00382-012-1387-z

Hohenegger C, Brockhaus P, Schaer C (2008) Towards climate simulations at cloud-resolving scales. Meteorolo Z 17(4):383–394

Jacob D, Petersen J, Eggert B, Alias A, Christensen OB, Bouwer LM, Braun A, Colette A, Déqué M, Georgievski G (2014) EURO-CORDEX: new high-resolution climate change projections for european impact research. Reg Environ Change 14(2):563–578. doi:10.1007/s10113-013-0499-2

Jones RG, Murphy JM, Noguer M (1995) Simulation of climate change over Europe using a nested regional-climate model. I: assessment of control climate, including sensitivity to location of lateral boundaries. Q J Roy Meteorol Soc 121(526):1413–1449

Kain JS, Fritsch JM (1990) A one-dimensional entraining/detraining plume model and its application in convective parameterization. J Atmos Sci 47(23):2784–2802

Kendon EJ, Roberts NM, Senior CA, Roberts MJ (2012) Realism of rainfall in a very high-resolution regional climate model. J Clim 25(17):5791–5806. doi:10.1175/JCLI-D-11-00562.1

Kendon EJ, Roberts NM, Fowler HJ, Roberts MJ, Chan SC, Senior CA (2014) Heavier summer downpours with climate change revealed by weather forecast resolution model. Nat Clim Change. doi:10.1038/nclimate2258

Kjellström E, Fowler HJ, Kendon EJ, Leung R, Truhetz H (2014) Taking the next step towards very-high-resolution regional climate modeling. GEWEX News 24(3):4–5

Kuo HL (1965) On formation and intensification of tropical cyclones through latent heat release by cumulus convection. J Atmos Sci 22(1):40–63

Laprise R (1992) The Euler equations of motion with hydrostatic pressure as an independent variable. Mon Weather Rev 120(1):197–207

Lauwaet D, Viaene P, Brisson E, van Noije T, Strunk A, Van Looy S, Maiheu B, Veldeman N, Blyth L, De Ridder K (2013) Impact of nesting resolution jump on dynamical downscaling ozone concentrations over Belgium. Atmos Environ 67:46–52

Leduc M, Laprise R (2009) Regional climate model sensitivity to domain size. Clim Dyn 32(6):833–854. doi:10.1007/s00382-008-0400-z

Leduc M, Laprise R, Moretti-Poisson M, Morin JP (2011) Sensitivity to domain size of mid-latitude summer simulations with a regional climate model. Clim Dyn 37(1–2):343–356. doi:10.1007/s00382-011-1008-2

Li J, Barker HW (2005) A radiation algorithm with correlated-k distribution. Part I: local thermal equilibrium. J Atmos Sci 62(2):286–309

Martynov A, Laprise R, Sushama L, Winger K, Šeparović L, Dugas B (2013) Reanalysis-driven climate simulation over CORDEX North America domain using the Canadian Regional Climate Model, version 5: model performance evaluation. Clim Dyn. doi:10.1007/s00382-013-1778-9

McFarlane NA (1987) The effect of orographically excited gravity wave drag on the general circulation of the lower stratosphere and troposphere. J Atmos Sci 44(14):1775–1800

Pavlik D, Söhl D, Pluntke T, Mykhnovych A, Bernhofer C (2012) Dynamic downscaling of global climate projections for eastern Europe with a horizontal resolution of 7 km. Environ Earth Sci 65(5):1475–1482. doi:10.1007/s12665-011-1081-1

Prein AF, Langhans W, Fosser G, Ferrone A, Ban N, Goergen K, Keller M, Tlle M, Gutjahr O, Feser F (2015) A review on regional convectionpermitting climate modeling: demonstrations, prospects, and challenges. Rev Geophys. doi:10.1002/2014RG000475

Rasmussen R, Liu C, Ikeda K, Gochis D, Yates D, Chen F, Tewari M, Barlage M, Dudhia J, Yu W (2011) High-resolution coupled climate runoff simulations of seasonal snowfall over Colorado: a process study of current and warmer climate. J Clim 24(12):3015–3048. doi:10.1175/2010JCLI3985.1

Šeparović L, Alexandru A, Laprise R, Martynov A, Sushama L, Winger K, Tete K, Valin M (2013) Present climate and climate change over North America as simulated by the fifth-generation Canadian regional climate model. Clim Dyn 41(11–12):3167–3201. doi:10.1007/s00382-013-1737-5

Skamarock WC (2004) Evaluating mesoscale NWP models using kinetic energy spectra. Mon Weather Rev 132(12):3019–3032. doi:10.1175/MWR2830.1

Sundqvist H, Berge E, Kristjánsson JE (1989) Condensation and cloud parameterization studies with a mesoscale numerical weather prediction model. Mon Weather Rev 117(8):1641–1657

Taylor KE (2001) Summarizing multiple aspects of model performance in a single diagram. J Geophys Res Atmos (1984–2012) 106(D7):7183–7192

Trapp RJ, Halvorson BA, Diffenbaugh NS (2007) Telescoping, multimodel approaches to evaluate extreme convective weather under future climates. J Geophys Res Atmos (1984–2012) 112:D20109. doi:10.1029/2006JD008345

Verseghy DL (2000) The Canadian land surface scheme (CLASS): its history and future. Atmos Ocean 38(1):1–13

Verseghy L (2008) The Canadian land surface scheme: technical documentation-version 3.4. Climate Research Division, Science and Technology Branch, Environment Canada

Von Storch H, Langenberg H, Feser F (2000) A spectral nudging technique for dynamical downscaling purposes. Mon Weather Rev 128:3664–3673

Vries H, Lenderink G, Meijgaard E (2014) Future snowfall in western and central europe projected with a highresolution regional climate model ensemble. Geophys Res Lett 41(12):4294–4299

Wang C, Jones R, Perry M, Johnson C, Clark P (2013) Using an ultra-high-resolution regional climate model to predict local climatology. Q J Roy Meteorol Soc 139(677):1964–1976. doi:10.1002/qj.2081

Yeh KS, Côté J, Gravel S, Méthot A, Patoine A, Roch M, Staniforth A (2002) The CMC-MRB global environmental multiscale (GEM) model. Part III: nonhydrostatic formulation. Mon Weather Rev 130(2):339–356

Zadra A, Roch M, Laroche S, Charron M (2003) The subgridscale orographic blocking parametrization of the GEM model. Atmos Ocean 41(2):155–170